Point defect geometries in inverted opal photonic crystals

David L. C. Chan, E. Lidorikis, and J. D. Joannopoulos
Department of Physics and Center for Materials Science and Engineering, Massachusetts Institute of Technology, Cambridge, Massachusetts 02139, USA
(Received 25 June 2004; published 5 May 2005)

We study point defect geometries in inverted opal photonic crystals that can be easily fabricated by means of colloidal self-assembly. Two broad classes of defects are considered: substitutional and interstitial. Substitutional point defects are found to introduce a usable defect band into the photonic band gap. This can be done by using a silica sphere of radius between $0.33a$ and $0.35a$ (where a is the lattice constant). The state is triply degenerate. Reflectance and local density of states calculations are performed to verify the existence and frequency of this defect. The point defect can be made by precoating shrunk silica spheres with a thin layer of silicon. Such a defect can be used as a microcavity for localizing light at a point, with a quality factor Q that is limited primarily by the proximity of the defect to the surface of the photonic crystal and other such defects.

DOI: 10.1103/PhysRevE.71.056602 PACS number(s): 42.70.Qs, 61.72.Ji, 72.10.Fk

I. INTRODUCTION

Recently, there has been much interest in fabricating photonic crystals by means of colloidal self-assembly [1–8]. Such a method is attractive because it offers a simpler and cheaper way of making three-dimensionally (3D) periodic photonic crystals, compared with conventional semiconductor nanofabrication techniques. Work has been done to show that self-organizing systems that self-assemble into large-scale photonic crystals can have photonic band gaps (PBGs) or pseudogaps in the near-visible frequency regime [9–21]. Natural assembly of colloidal microspheres yields irregular, polycrystalline photonic crystals with many structural defects that can destroy the PBG. However, it turns out that strong capillary forces at a meniscus between a substrate and a colloidal sol can induce crystallization of spheres into a 3D array of controllable thickness. Sweeping this meniscus slowly across a vertically placed substrate by solvent evaporation leads to the deposition of thin planar opals. This technique has been used by Vlasov *et al.* [2] to produce inverted opal photonic crystals with band gaps at around 1.3 μm.

Deliberately designed defects are desirable features in photonic crystals [22,23]. A point defect, for example, with a mode localized within a complete PBG would give rise to a microcavity, while a line defect can be used as a waveguide [1,24]. Microcavities and waveguides can be used as building blocks for optical devices and all-optical integrated circuits. There is, therefore, a need to design defects that can exist in the gap and be easily introduced into the bulk structure. Since colloidal self-assembly appears to be a promising and economical way of fabricating photonic crystals, we would like to identify a class of point defects that can be made using this method. This was the motivation for the work described in this paper. Computational calculations for such systems are of great importance because they can serve as a prelaboratory where different ideas of possible defect geometries are tested and refined. One can have faith in relatively accurate correspondence between calculation and experiment, since Maxwell's equations are essentially exact in the linear regime of low photon-photon coupling, the regime in which such crystals are used.

II. POINT DEFECT GEOMETRIES

We consider an inverted opal structure, which is a face-centered cubic lattice of air spheres in a silicon background. Such a structure can be thought of as the *inverse* of the more familiar fcc crystal of silicon spheres in air. Experimentally, synthetic opals can be made by colloidal crystallization of a fcc lattice of silica spheres, backfilling interstitial spaces with silicon, and then wet-etching out the silica spheres, leaving air spheres behind. However, the infiltration of the background with silicon is usually imperfect, leaving some air gaps in between the silica spheres. We take this imperfection into account in our simulations by building up the structure using air spheres with a $0.06a$ (where a is the lattice constant of the fcc lattice; in all that follows, length scales will be given in units of a) coating of silicon, which leaves air gaps in the diagonal spaces between spheres. In the structure under study, the air spheres have a radius of $0.354a$, so the silicon coating is about 17% of the radius of the air spheres. The air spheres are overlapping because the critical radius for the overlap of spheres in fcc crystals is $a/(2\sqrt{2}) = 0.354a$. We terminate the surface using a plane that cuts the spheres in half, because this appears to be more similar to what is produced in experiments by Vlasov *et al.*

In general, one can create a defect by adding or removing dielectric. The former method produces a *dielectric* defect while the latter gives an *air* defect [25]. Both are effective ways of introducing defects to a photonic crystal system, though there are connectivity issues that make the two methods different, depending on whether the crystal itself is dielectric or air connected (or both). It should also be noted that the orientation of the crystal can affect the reflectance measurements. It turns out that, for inverted opals, samples of higher quality can be obtained with surfaces normal to the [111] direction than to the [100] direction. For this reason, most of our work involves studying crystals with [111] surface orientation. Furthermore, in experimental measurements, the wafer was placed on top of a silicon substrate. It was thought that the presence of the substrate could have a nontrivial effect on reflectance measurements. However, hav-

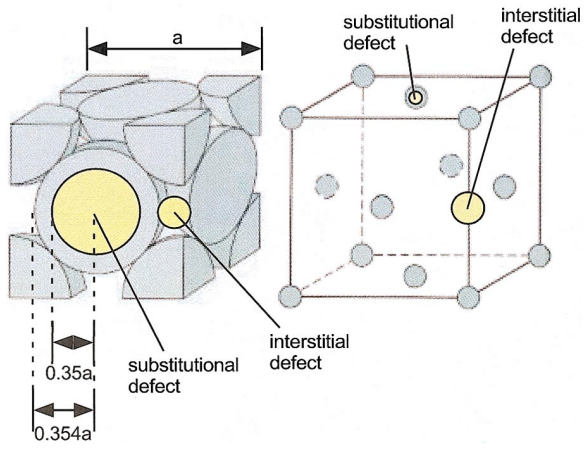

FIG. 1. (Color) Two different styles of point defects (adapted from [26]).

ing performed calculations with and without the substrate, we find no significant differences.

Figure 1 shows the two different defect geometries that we considered. An interstitial defect is designed to fit into the spaces between the larger spheres. A substitutional defect replaces an existing sphere.

In the interstitial case, it is necessary that these interstitial spheres be sufficiently small; otherwise, their presence in the colloidal self-assembly process would disrupt the structure of the rest of the crystal. The upper bound on the radius of the small sphere is $(1/2)(1-1/\sqrt{2})a \approx 0.146a$. Single interstitial air and dielectric defects can be implemented by having small silica or silicon spheres, and were tried in our calculations. We also considered clumps of seven or eight such air and dielectric defects. The presence of interstitial air defects changes the connectivity of the system, since new air channels have been created joining nonadjacent large air spheres. Interstitial dielectric spheres, however, only affect the system insofar as they fill in the "holes" that were not completely backfilled with silicon. In any case, our results for these interstitial defect geometries revealed no particularly useful change in the band structure of these systems that could lead to the existence of a defect band in the gap. The change tended to either pull down some states from the upper bands into the gap, but only for certain wave vectors, or destroy the photonic band gap altogether. In the remainder of this paper, we will restrict our attention to substitutional defects.

In the substitutional case, the outer radius must lie between $0.146a$ and $0.354a$: if less than the former, then the sphere will slide into an interstitial space; if greater than the latter, it will disrupt the packing of the structure. A relatively easy modification would be to reduce the size of the silica spheres used to create the structure. Note, however, that if the radius of the silica spheres is decreased below $0.354a$, the defect sphere will no longer be touching adjacent, normal spheres. This means that after backfilling, the defect sphere will be completely enclosed by silicon, and the silica material inside will *not* be etched away by the wet-etching process. We have effectively created a defect sphere with silica ($\epsilon = 2.1025$) inside instead of air, amounting to a dielectric substitutional defect. We study this class of defects for different radii of silica spheres, and identify some useful properties.

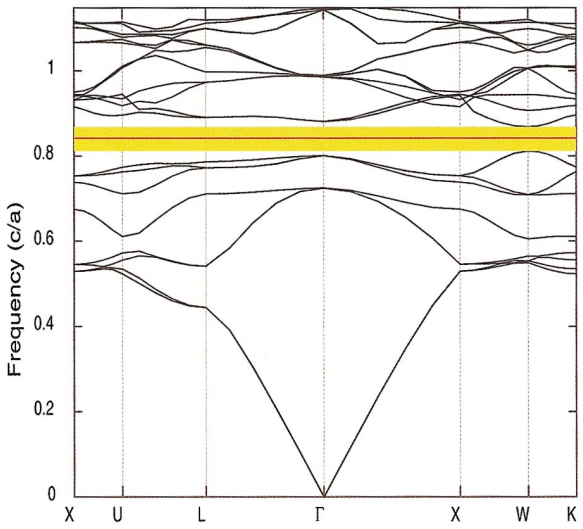

FIG. 2. (Color) Band structure of photonic crystal with point defect mode. Defect calculation performed with $3\times3\times3$ supercell, with a (48,48,48) basis set, for shrunk silica sphere radius of $0.35a$. The $3\times3\times3$ supercell calculation for the defect-produced band structure with multiple folding of bands, and as such the band diagram for that calculation is not edifying to show. The most important result from that calculation, namely, the defect state frequency, was extracted, and this piece of information was incorporated into the above nonsupercell band structure.

III. CHARACTERISTICS OF THE DEFECT STATE

To determine the properties of a photonic crystal structure, it is important to be able to calculate its band structure and reflectance spectrum, since the first tells us about the modes the structure supports, and the second allows us to make direct comparison with experimental results. We calculate band structure using the MIT PHOTONIC BANDS program, which uses a variational method to solve the Maxwell eigenvalue equation [24]. For reflectance, we perform a time domain simulation of the fields using a finite difference technique. Note that in both our frequency and time domain calculations, we did not allow frequency to go above 1.0 (in units of c/a) because we did not wish to concern ourselves with diffraction. By working with frequencies below 1.0, a normally incident light wave would produce a transmitted wave that is also normal. For frequencies above 1.0, several diffracted beams are possible, corresponding to different wave vectors, which are conserved by the scattering of the photonic crystal only up to a reciprocal lattice vector. Thus, we have reduced the problem to a one-dimensional one. Such a simplification is acceptable, given that the experimental measurements of Vlasov *et al.* were mostly at 1.0 or below.

Figure 2 shows the band structure of a system with a shrunk silica sphere of radius $0.35a$. The bands for the bulk structure were calculated using a basis set ranging from (8,8,8) to (256,256,256), and (16,16,16) was found to be ef-

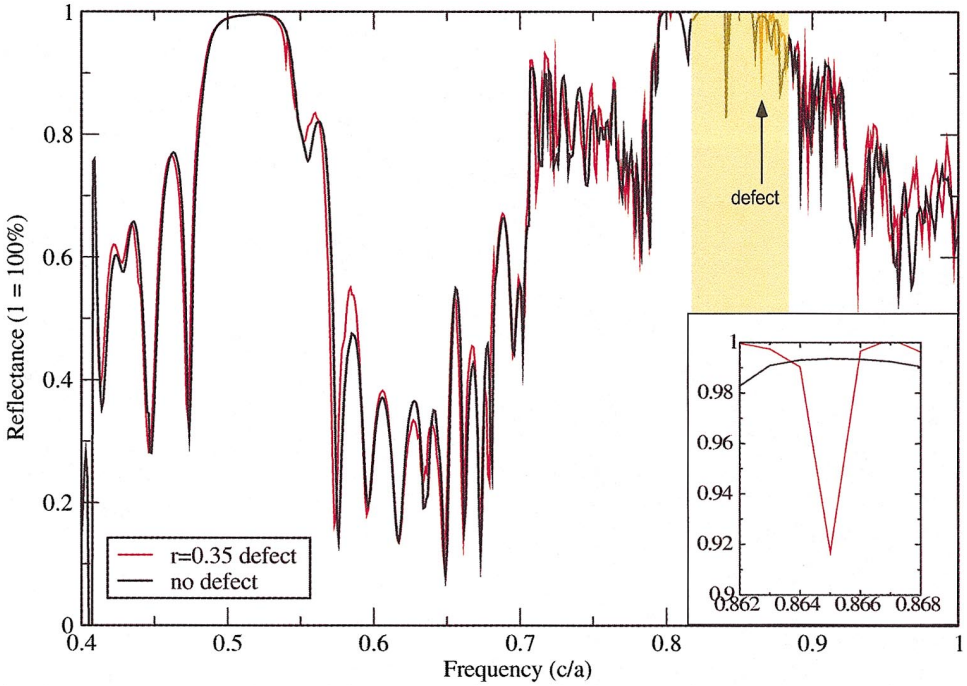

FIG. 3. (Color) Reflectance spectrum of photonic crystal, with and without point defect. The dipole source is polarized in the [110] direction. The computational cell used had dimensions of $56\times97\times411$ grid points, corresponding to 40 grid points per lattice constant. The photonic crystal slab was seated on a silicon substrate. A 2×2 supercell was used, and the simulation was run for 79 195 time steps. (Inset shows magnified version of reflectance dip due to defect.)

fectively converged. The defect band was calculated by introducing the defect into the system and performing the calculation with a $3\times3\times3$ supercell and a basis set of (48,48,48). A supercell calculation was required in this case because the presence of the defect *reduced* the periodicity of the structure, and resulted in an *increase* of the size of the repeating cell. Ideally, we would use an isolated defect in an otherwise periodic crystal, but it turns out that having a periodic system simplifies the calculations enormously, as it allows us to impose periodic boundary conditions and apply Bloch's theorem. The choice of the size of the supercell involves striking a balance between preventing excessive coupling between defects in adjacent supercells (this is equivalent to requiring a high-Q cavity), and computation time. The first consideration leads us to increase the size of the supercell while the second leads us to decrease it. It was found that $3\times3\times3$ gave good results for band structure calculations without incurring unacceptably long computation times. We see from the figure that the presence of the defect pulled down some of the upper bands to the middle of the gap while maintaining the overall integrity of the PBG. This geometry has the desirable features that we look for.

We also performed band structure calculations for shrunk silica spheres of different radii. We examined a series of defect radii from $0.15a$ to $0.35a$. Each one of these defect radii produces a change in the band structure of the system. The defect pulls down some states from above the gap. The larger the radius, the further into the gap the states are pulled. Since we are interested in the local confinement of light, and such confinement requires the existence of defect bands within an otherwise forbidden region, we are looking for radii that pull down states such that they are in or near the middle of the gap with forbidden regions on either side. It turns out that such a defect state can be produced with defect radii between $0.33a$ and $0.35a$. Obviously, the smaller the radius, the greater the overall increase in dielectric constant. In general, the frequency of the defect mode decreases as the average dielectric constant of the defect is increased; this is the qualitative dependence of defect frequency on dielectric constant. We show $0.35a$, which is the defect mode that is most easily distinguished from the surrounding background of states. We did a careful counting of the number of defect bands pulled down by the defect into the gap, and it turns out to be three. Thus, the defect state is triply degenerate. (Such a result is certainly consistent given the cubic symmetry of the lattice.) The symmetry of the defect structure allows for a threefold degenerate irreducible representation, which in turn leads to a threefold degenerate state.

As an aside, it is useful to observe that the adequacy of a particular size of supercell for the calculation at hand can be determined from the flatness of the defect band. A point defect has complete directional symmetry and its mode must therefore be independent of wave vector. This corresponds to a flat band in ω-k space. If the supercell is insufficiently large, the defects would be interacting (in a tight-binding sense), and such interaction would produce a network of interlinked defects, favoring the {100}, or cubic, directions. In other words, the band would not be flat. We were able to have confidence in the frequency of the defect band to the extent that the bands obtained in our $3\times3\times3$ supercell calculations were acceptably flat.

Figure 3 gives the reflectance spectrum for the system with and without the defect. The computational cell chosen was a long one, with dimensions $56\times97\times411$ grid points, corresponding to about 40 grid points per lattice constant a. The photonic crystal slab was in the middle, and flux planes were placed on either side of it at distances of $1.5a$ and $4a$. The slab was nine spheres thick, seated on a silicon substrate, and the surface was normal to the [111] direction. This was also a supercell calculation, though in this case, we used a 2×2 supercell because we wanted to produce a wider band and stronger coupling of the incident radiation with the de-

fect mode. In these computational experiments, a dipole source was used instead of a Gaussian plane wave, as the former contains many different wave vectors while the latter contains only one (that which corresponds to normal incidence), and we want the incident radiation to couple into the defect mode, irrespective of its symmetry. The simulation was run for a total of 79 195 time steps. This was chosen to be sufficiently large to ensure that the Gaussian pulse had sufficient time to propagate through the entire system. The reflectance was calculated by the following equation, which comes from dividing the magnitude of the reflected flux ($|\mathbf{E}^{\text{slab}}-\mathbf{E}^{\text{vac}}|^2$) by the magnitude of the incident flux ($|\mathbf{E}^{\text{vac}}|^2$):

$$R=\frac{|E_x^{\text{slab}}-E_x^{\text{vac}}|^2+|E_y^{\text{slab}}-E_y^{\text{vac}}|^2+|E_z^{\text{slab}}-E_z^{\text{vac}}|^2}{|E_x^{\text{vac}}|^2+|E_y^{\text{vac}}|^2+|E_z^{\text{vac}}|^2}.$$

Note that all fields are functions of frequency, for a given point in space, as we take the Fourier transform of the time series of fields in real time. A discrete Fourier transform was performed on the entire time series, and no averaging was required. We take the absolute values because the fields are complex quantities in general. We run the simulation once with the slab in place, and then again with vacuum only, and the difference in fields between the first run and the second run, when expressed as a fraction of the intensities in the vacuum case, gives the reflectance. For normally incident radiation, one only needs to record the fields at one monitor point situated between the source plane and the slab, but for a dipole source, integration over a flux plane is required since the fields are different in different directions. That is what we did to obtain Fig. 3.

One can see good agreement between the black curve (no defect) and the red curve (defect) at almost all frequencies. To find the effect of the point defect, we focus our attention on the region of the photonic band gap. This is a region where we expect near 100% reflectance, since there are no propagating modes within the slab for that range of frequencies, and the slab is thick enough to prevent tunneling of evanescent waves. It is encouraging to see the reflectance dip caused by the point defect, which has been highlighted along with the band gap region. The position of the dip agrees with the frequency of the defect state predicted by the band structure calculations. We stress that the band structure and reflectance spectrum are two different calculations, and that the agreement between the two on the frequency of the defect mode is a strong indication of the reliability of our results.

The introduction of a defect causes a redistribution of the local density of states (LDOS) of the system, with the total number of states being conserved. The defect takes a few states from outside the gap and puts them inside the gap. This change is localized in space but not in frequency. Integrating the LDOS over all volume (including the defect) gives the global density of states. If the total number of states in the system is N, then the effect of the defect is to put a state of weight ~ 1 in the gap and reduce the DOS outside the gap by $\sim 1/N$. Transmission as a function of frequency is proportional to the global density of states. In a structure of infinite extent, $N\rightarrow\infty$ and the change in DOS outside the gap tends to zero. However, in such a limit, the defect state becomes unobservable because $1 \ll N$. Thus, a compromise is needed to keep the disturbance to states outside the gap small while allowing the localized state to have an observable effect on the spectrum inside the gap. This is also the reason why it is impossible to observe the defect mode in a reflectance spectrum without collateral change to the spectrum outside the gap (though the relative magnitudes of these changes are in the ratio $1:1/N$).

We recognize also that there are a few reflectance dips *within* the photonic band gap that appear to be states inside the gap. On closer examination, however, one can see that the black and red curves overlap completely for these "states." What this means is that the dips are present irrespective of the existence of the defect. We understand these to be resonant transmission peaks caused by the finite size of the photonic crystal slab that we used in our calculations. Therefore, they are *not* localized states.

We also point out that while a dipole source contains many wave vectors, in practice, because of the long computational cell and the distance between the source and the slab, the light that reaches the slab is not too far from being normally incident. As a result, the light hits the slab with a wave vector close to the Γ-L direction (111). The band structure calculation (Fig. 2) exhibits a partial gap in the Γ-L direction between 0.45 and 0.55, and we see this showing up in the reflectance spectrum in the form of a region of high reflectance between 0.48 and 0.55. The range of frequencies does not correspond exactly because the incidence is only approximately normal. Similarly, we see a region of high (but not unity) reflectance between 0.7 and 0.77, corresponding to the partial Γ-L gap in that range.

To obtain even more definite evidence of the existence and frequency of the defect state, we performed calculations of the local density of states of the photonic crystal system, and these results are presented in Fig. 4. The local density of states of a system is defined by

$$D(\omega,\mathbf{r})=\sum_{n\mathbf{k}}|E_{n\mathbf{k}}(\mathbf{r})|^2\delta(\omega-\omega_{n\mathbf{k}})$$

such that

$$D(\omega)=\int D(\omega,\mathbf{r})d^3\mathbf{r}=\sum_{n\mathbf{k}}\int|E_{n\mathbf{k}}(\mathbf{r})|^2\delta(\omega-\omega_{n\mathbf{k}})d^3\mathbf{r}$$
$$=\sum_{n\mathbf{k}}\delta(\omega-\omega_{n\mathbf{k}})$$

where $D(\omega)$ is the *global* density of states, and $E_{n\mathbf{k}}(\mathbf{r})$ is assumed to be normalized to unity over all space. We see that integrating the local density of states over all space gives the global density of states, as required.

Such a calculation can be done numerically by integrating over "shells" of constant energy in k space [27,28]:

$$D(\omega,\mathbf{r})=2\frac{V}{(2\pi)^3}\int\frac{dS_\omega}{v_g}$$

where $v_g=|\nabla_{\mathbf{k}}\omega(\mathbf{k})|$, the magnitude of the group velocity, and the integral is performed over a surface of constant energy $\omega(\mathbf{k})$. The extra factor of 2 accounts for the two trans-

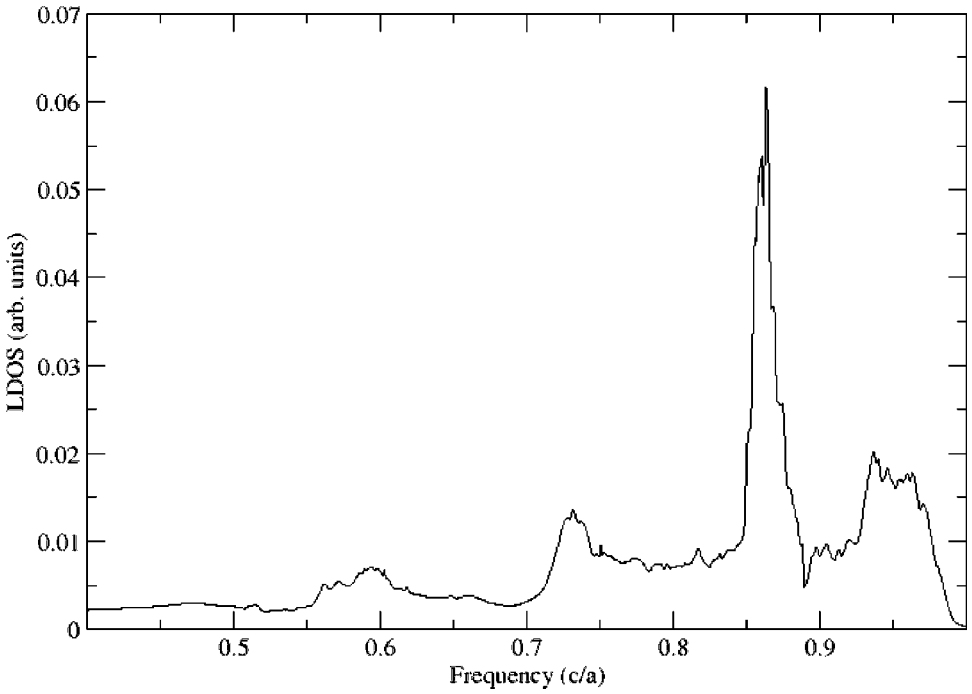

FIG. 4. Local density of states of photonic crystal, with point defect. We followed the Gilat-Raubenheimer method, using eight evenly spaced k points in the irreducible Brillouin zone.

verse polarizations of light. The local density of states can be thought of as the probability of finding a photon with frequency ω at point $\mathbf{r}$, irrespective of wave vector or band number (these are summed over). We choose to calculate the local density of states for a point near the center of the defect sphere, with the physical understanding that if a defect mode exists, it should have a mode profile that has a high concentration of photons within the defect sphere. We therefore expect a peak at around $0.86c/a$ in the LDOS spectrum. Numerically, we follow the Gilat-Raubenheimer method [29,30] of dividing up the irreducible Brillouin zone into a cubic mesh and approximating the constant energy surface with parallel planes. We use eight evenly spaced k points in the irreducible Brillouin zone. Another way of doing it would be to use a special k-point scheme [31].

Our local density of states calculation exhibits a very distinct peak at about $0.86c/a$, showing clearly the existence of the defect mode. The LDOS is low for frequencies on either side of the peak because of the photonic band gap. However, it is not zero because our LDOS calculation was performed on a slab rather than an infinite structure. The band structure calculation was done on an infinite crystal and so it had a real gap. A slab, on the other hand, only has a pseudogap, and so we see some states inside the pseudogap region. (Incidentally, we chose to do the calculation for a slab because that is what can be made and observed experimentally.) Therefore, we do not expect zero LDOS in the "gap" region. The frequency of the peak agrees well with our band structure predictions and reflectance calculations. There are interesting peaks on either side of the main defect peak. They show that the defect produces resonant structure beyond the gap. These resonant structures are more noticeable with a finite slab than an infinite one in which the resonances wash out.

IV. CONCLUSION

In this work, we studied possible point defect geometries in inverted opal photonic crystals that can be easily fabricated by means of colloidal self-assembly. Two broad classes of defects were considered: interstitial and substitutional. Calculations for isolated as well as clumps of interstitial defects did not reveal promising changes to the band structure that could introduce a defect band into the photonic band gap. On the other hand, substitutional defects, wherein the air sphere is replaced by a smaller silica sphere surrounded by silicon, were found to be much more promising. By performing high-resolution band structure calculations, we were able to determine that a silica sphere of radius between $0.33a$ and $0.35a$ could introduce a clear and usable defect mode into the gap. The state is found to be triply degenerate. We are encouraged by the results of our band structure, reflectance, and local density of states calculations, all of which agree on the frequency of the defect mode. Since these are three different calculations, we have confidence that the defect mode exists.

The proposed defect can be made by replacing some of the $0.354a$ silica spheres with $0.35a$ spheres in the colloidal self-assembly process. Backfilling the assembled structure with silicon should result in a thicker coating of silicon for the shrunk spheres than for the normal ones, yielding the geometry we put forward in this paper. One possible problem with this approach, however, is that the smaller silica sphere is unlikely to be "floating" between other spheres and might quite possibly be touching one of the larger spheres around it. This could prevent complete coating of the silica sphere during the backfill. If there is a silica-silica point of contact between the shrunk sphere and an adjacent sphere, then the wet-etching process could remove the silica from the defect sphere as well. One way of overcoming this problem would

be to precoat the shrunk silica spheres with silicon. The ideal situation would be to have the $0.35a$ silica spheres coated with a layer of silicon that is $0.004a$ thick, resulting in a total radius of $0.354a$ for the "hybrid" sphere. We can vary the density of such hybrid spheres in order to tune the Q value of the cavities. The higher the concentration, the smaller the effective supercell, and the stronger the coupling of radiation with the mode.

ACKNOWLEDGMENTS

We thank David Norris and Yurii Vlasov for introducing us to this problem. We also thank our colleagues Peter Bermel and David Roundy at the Massachusetts Institute of Technology for helpful discussions. This work was supported in part by the Croucher Foundation, Hong Kong, and the MRSEC program of the NSF under Grant No. DMR-0213282.

[1] J. D. Joannopoulos, P. R. Villeneuve, and S. Fan, Nature (London) **386**, 143 (1997).
[2] Y. A. Vlasov, X.-Z. Bo, J. C. Sturm, and D. J. Norris, Nature (London) **414**, 289 (2001).
[3] J. D. Joannopoulos, Nature (London) **414**, 257 (2001).
[4] Y. A. Vlasov *et al.*, Phys. Rev. E **61**, 5784 (2000).
[5] B. A. Parviz, D. Ryan, and G. M. Whitesides, IEEE Trans. Adv. Packag. **26**, 233 (2003).
[6] O. E. Rogach *et al.*, Mater. Sci. Eng., B **64**, 64 (1999).
[7] F. Bresson *et al.*, Appl. Surf. Sci. **217**, 281 (2003).
[8] J. R. Link and M. J. Sailor, Proc. Natl. Acad. Sci. U.S.A. **100**, 10 607 (2003).
[9] K. Busch and S. John, Phys. Rev. E **58**, 3896 (1998).
[10] A. Blanco *et al.*, Nature (London) **405**, 437 (2000).
[11] Y. Saado, M. Golosovsky, D. Davidov, and A. Frenkel, Phys. Rev. B **66**, 195108 (2002).
[12] Z. Wang, C. T. Chan, W. Zhang, N. Ming, and P. Sheng, Phys. Rev. B **64**, 113108 (2001).
[13] L. Martin-Moreno, F. J. Garcia-Vidal, and A. M. Somoza, Phys. Rev. Lett. **83**, 73 (1999).
[14] R. D. Pradhan, J. A. Bloodgood, and G. H. Watson, Phys. Rev. B **55**, 9503 (1999).
[15] S. John and K. Busch, J. Lightwave Technol. **17**, 1931 (1999).
[16] A. F. Koenderink, L. Bechger, H. P. Schriemer, A. Lagendijk, and W. L. Vos, Phys. Rev. Lett. **88**, 143903 (2002).
[17] P. M. Johnson, A. F. Koenderink, and W. L. Vos, Phys. Rev. B **66**, 081102(R) (2002).
[18] H. P. Schriemer, H. M. van Driel, A. F. Koenderink, and W. L. Vos, Phys. Rev. A **63**, 011801(R) (2000).
[19] B. Li *et al.*, Appl. Phys. Lett. **82**, 3617 (2003).
[20] V. N. Astratov *et al.*, Phys. Rev. B **66**, 165215 (2002).
[21] V. Yannopapas, N. Stefanou, and A. Modinos, Phys. Rev. Lett. **86**, 4811 (2001).
[22] M. H. Qi *et al.*, Nature (London) **429**, 538 (2004).
[23] T. D. Happ, M. Kamp, and A. Forchel, J. Opt. Soc. Am. B **20**, 373 (2003).
[24] S. G. Johnson and J. D. Joannopoulos, *Photonic Crystals: The Road from Theory to Practice* (Kluwer, Dordrecht, 2002).
[25] J. D. Joannopoulos, R. D. Meade, and J. N. Winn, *Photonic Crystals: Molding the Flow of Light* (Princeton University Press, Princeton, NJ, 1995).
[26] W. D. Callister, *Fundamentals of Materials Science and Engineering: An Interactive e-Text* (Wiley, New York, 2000).
[27] C. Kittel, *Introduction to Solid State Physics*, 7th ed. (Wiley, New York, 1996).
[28] N. W. Ashcroft and N. D. Mermin, *Solid State Physics* (Harcourt, Brace, Jovanovich, San Diego, 1976).
[29] G. Gilat and L. J. Raubenheimer, Phys. Rev. **144**, 390 (1966).
[30] L. J. Raubenheimer and G. Gilat, Phys. Rev. **157**, 586 (1967).
[31] H. J. Monkhorst and J. D. Pack, Phys. Rev. B **13**, 5188 (1976).